

Installation and Experiments of Visual Space Sensing Underwater Robot -BlueRov2-

Fumiya Yamaoka^{1†}, Renya Takahashi², Horng-Yi Hsu³, Yuichiro Toda⁴ and Mamoru Minami⁵

¹Graduate School of Natural Science and Technology, Okayama University
3-1-1 Tsushima-naka, Kita-ku, Okayama 700-8530, Japan
(Tel: +81-2-000-0000; E-mail: 0000@xxx.ac.jp)

Abstract: Recently, a number of researches related to underwater vehicle has been conducted worldwide with the huge demand in different applications. In the previous study, we proposed an underwater robot vision servo using a compound eye camera. 3D Model-based Matching Method is proposed for real-time attitude tracking applied to autonomous underwater vehicles (AUV). Real-time Multi-step Genetic Algorithm (RM-GA) is utilized in searching process of pose in term of optimization, because of its effectiveness, simplicity and promising performance of recursive evaluation, for real-time pose tracking performance. The proposed system is implemented as software implementation and Remotely Operated Vehicle (ROV) is used as a test-bed. In the simulation experiment, visual servo experiment in which the underwater robot recognized the target, estimated the relative attitude on the basis of the proposed system, and controlled it to the desired attitude, and docking experiment on the assumption of the automatic power supply from the submarine power supply equipment in the actual sea area were carried out.

Keywords: visual servoing, stereo camera, genetic algorithm, underwater vehicle, model-based recognition

1. INTRODUCTION

Nowadays, visual servoing in which visual information is used to control the robot's motion plays an important role in different domains of application with the rapid progresses in computer vision technology. Generally, visual servoing techniques are divided into two categories; Image-Based Visual Servoing (IBVS) and Position-Based Visual Servoing (PBVS). In IBVS techniques, images from camera are used directly for control of robot. In PBVS, information of known object are extracted and interpreted from the images and used in controlling of robot in reference space rather than in image space as in IBVS [1-3]. Based on the location of camera, eye-in-hand and eye-to-hand configuration are considered according to the requirement of application. Then, the techniques are differentiated based on the number of cameras; from single to multi cameras. Even though there are some limitations for real-time applications in terms of image-acquisition-quantization accuracy and processing rates, the role of visual information has been expanding rapidly in industry and society in line with efforts of researchers [4, 5].

Like the land and space systems, a number of researches on underwater vehicle using visual servoing has been conducted worldwide recently [6-25]. Each of them is with different merits and limitations. Most of researches are based on the monocular vision [6, 7]. In [8], vision system using artificial underwater landmarks in order to be able to act autonomously using two cameras was reported. In the contribution of [9], features in plate are extracted and relative pose is estimated using the oriented FAST and rotated BRIEF (ORB) feature extractor. Even though two cameras are equipped in [8, 9], only one of cameras is used to estimate the position and orientation of the target and another camera is for another task. There are some related works using stereo vision for underwater vehicle [10, 11]. In [10], a new approach of position measurement for underwater vehicle-



Fig. 1. Underwater robot and 3D marker.

manipulator systems using pan-tilt-slide cameras categorized in IBVS was proposed. Epipolar geometry calculation of target consisting of four LED is realized using slide mechanism. Combining monocular and binocular vision positioning algorithm was introduced in [11], reducing limitation of image matching technique using two cameras. In [11], dead reckoning algorithm was introduced as an aided navigation because of longer computing time for vision based navigation. Geometry calculation for relative position of target consisting of LED is used in both [10, 11]. So for our group has continued to construct visual control and docking system, using ROV that has many difficulties to deal with the control line connecting the ROV and computer system set on the ground ashore. The difficulties include that the line restrict the ROV's motions by inner forces and torques exerting to the ROV. Therefore we need to develop AUV that doesn't have any lines and can move freely, which frings us easier condition to control the vehicle pose. As we are thinking in this way, we have developed vision-based underwater vehicle using standalone dual-eyes cameras and 3D marker in PBVS that is passive target for real-time pose tracking as shown in Fig.1 The developed system estimates a relative position and orientation between ROV and target object using 3D model-based matching method utilizing RM-GA. It is shown experimentally that regulating experiment can be implemented using proposed system, approving its accuracy.

† Yamaoka Fumiya is the presenter of this paper.

2. PROPOSE SYSTEM

The basic concept of the vision-based control technology is to minimize an error that is represented by difference between image measurement and desired value. In proposed system[25], desired value is relative pose (position and orientation) of robot with respect to target in Cartesian space rather than in image space and image measurements are a set of 3D parameters from which current pose is estimated in real-time. The main task of this work is to control the underwater robot to be regulated in desired pose to the target by means of visual servoing. In this system, the images acquired from the dual-eyes cameras are sent to a PC. Then, the real-time 3D pose estimation of the target object is executed in software implementation of the PC. Finally, based on the error between target value and estimated value, command signals generated from calculating the voltage value gained by P controller for the thrusters are input into ROV in order to keep desired pose.

2.1. 3D Model-Based Matching Method

Instead of calculation of the absolute position of the vehicle and the target, the relative pose of the vehicle with respect to the known target is estimated using 3D modelbased recognition. In this method, knowing the information of the 3D marker and desired relative pose to the underwater vehicle, the solid model of the target is predefined and projected to 2D images. Then, the relative pose is calculated by comparing the projected solid model image with the captured 2D images by dual cameras.

Left and right cameras are mounted in vehicle in fixed and parallel position. Coordinate frames of image, camera, vehicle and model are defined as shown in Fig. 2. Searching area is assumed to be around the target. The relative pose between ROV and 3D marker is determined by six parameters $(x, y, z, \varepsilon_1, \varepsilon_2, \varepsilon_3)$, where the first three are position in Cartesian coordinate frame and the latter are orientation in Euler coordinate system represented by unit quaternion avoiding singularity issues [26].

Fig. 3 explains how to estimate the relative pose using 3D model-based matching method. Firstly, 3D marker models with different poses are initially set up in random within searching 3D space. The main task is to find the model that coincides exactly with the real 3D marker and then use the pose of that selected model as the estimated relative pose. To measure the matching degree, we define fitness function to be evaluated in 2D images. However, the number of all possible models within searching area is too huge for system to be evaluated with real-time performance. Therefore, we need optimization method to limit the number of models and generate new models until the best model is detected. In Fig. 3, it can be seen that a number of 3D models are initiated in random. Then, they are projected to 2D image planes of left and right cameras and matched with real target images using fitness value. Based on some fitter models, new models are generated until generated models approach to the real target. Finally, the best model is detected and the pose of detected model is selected as the estimated one. Note that this recog-

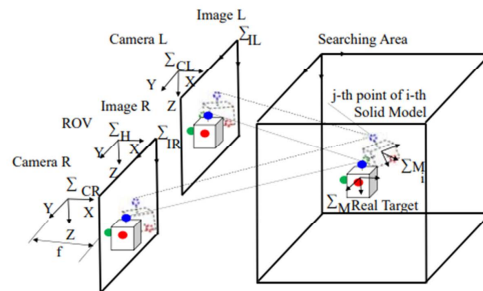


Fig. 2. Model-based pose estimation using dual-eyes vision system.

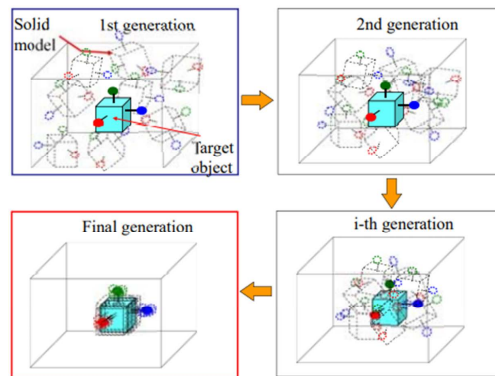


Fig. 3. 3D recognition process.



Fig. 4. 3D marker design.

niton process has to be performed within video rate (33 ms in our system).

2.1.1. 3D Marker

we developed the active 3D marker composed of red, yellow, green, and blue in each sphere. Fig. 4 shows the appearance of the active 3D marker. The 3D marker is constructed with a water proof box $(100 \times 100 \times 100[mm])$ and the spheres (diameter; $40[mm]$) are attached to the water proof box. The red, green and blue LEDs were installed into the spherical ball that is covered by the color balloon.

2.1.2. Fitness Function

To estimate the relative pose by comparing target object and object models, fitness value that is correlation function representing a matching degree of projected model against the real target in the image is used as the evaluation parameter. As shown in Fig. 5, there are two areas in model object to score fitness value namely; the inner one that is the same size

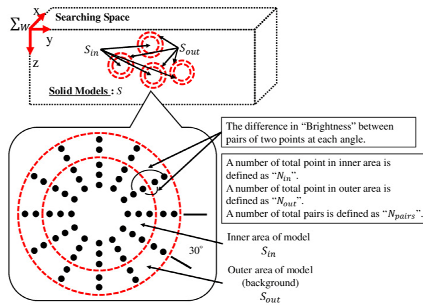


Fig. 5. Target and model object.

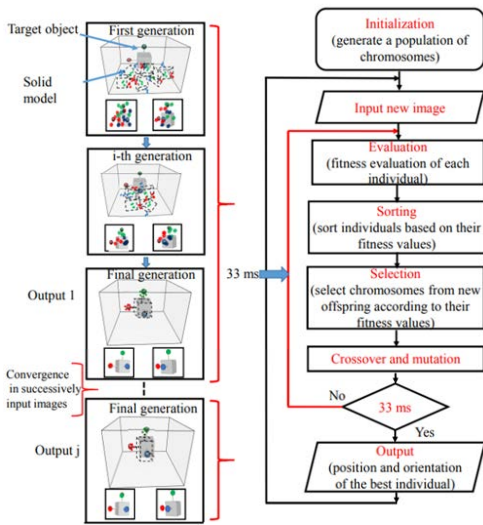


Fig. 6. Flowchart of RM-GA.

as the target sphere and the another one is background area. The portion of the captured target that lies inside the inner area of model will score up the fitness value and the portion that lies inside of the background area will score down the fitness value. It means the fitness value will be maximum when the target and the model are in coincidence. The overall fitness value is calculated from left image and right image. The detailed explanation can be seen in previous works [27-29].

2.2. RM-GA

In the process of the 3D pose estimation, it is assumed that there are many models in the search area, as shown in the left of Fig.6. In the right of Fig.6 shows the flowchart of the RM-GA and how the best model is obtained. The previous research [16] explained why and how the RM-GA developed for the real-time 3D pose estimation. For determining which model is closest to the actual target, the fitness function defined in the previous section was used to quantify the correlation between the models and the target. The main task of the pose estimation process is to search for the optimal model with the pose that is most strongly correlated with that of the real 3D marker.

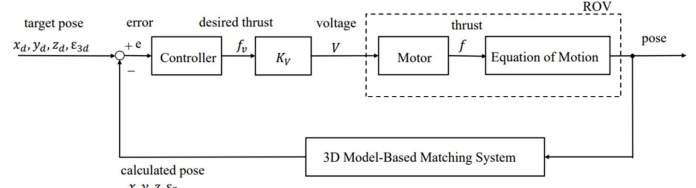


Fig. 7. Controllogic for the propose system.

2.3. Controller

To eliminate the error in relative pose to the target, Blue ROV's unique P control is used. Even though the proposed system estimates all six variables of pose, torque around x -axis and y -axis are neglected in control system because the x -axis and y -axis rotations are naturally restored to zero by the restoration torque made by the z -axis distance between the center of buoyance and the one of gravity. Therefore, only four degree of freedom is considered in control system. The proportional gain for each thruster is tuned according to the experimental results. The block diagram of the proposed control system is shown in Fig. 7.

Rotation

$$\text{(around } Z_H \text{ axis in Fig. 2)} : \nu_1 = k_{p1}(\epsilon_{3d} - \epsilon_3) + 2.5 \quad (1)$$

$$\text{Back and Force direction} \\ \text{(} X_H \text{ axis in Fig. 2)} : \nu_2 = k_{p2}(x_d - x) + 2.5 \quad (2)$$

$$\text{Left and right direction} \\ \text{(} Y_H \text{ axis in Fig. 2)} : \nu_3 = k_{p3}(y_d - y) + 2.5 \quad (3)$$

$$\text{Vertical direction} \\ \text{(} Z_H \text{ axis in Fig. 2)} : \nu_4 = k_{p4}(z_d - z) + 2.5 \quad (4)$$

where, ν_1 is input voltage for vertical thrusters for rotation movement of ROV around z -axis (Z_H in Fig. 2); ν_2 is input voltage for vectored thruster (shown in Fig. 8(a)(b)) for movement of ROV in back and forth direction (X_H in Fig. 2); ν_3 is input voltage for vectored thruster for movement of ROV in right and left direction (Y_H in Fig. 2), and ν_4 is input voltage for vertical thruster (shown in Fig. 8(d)) for movement of ROV in vertical direction (Z_H in Fig. 2). Note that the rotation of vehicle is controlled by four vectored thrusters that rotate in opposite direction.

2.4. Underwater Robot

Remotely controlled underwater robot used in this experiment (manufactured by BlueRobotics, maximum depth 100 m) is shown in Fig.8. Two fixed forward cameras with the same specification (imaging element CCD, pixel number 380,000 pixel, signal system NTSC, minimum illumination 0.0035 lx, no zoom) are mounted on ROV. The 2 fixed forward cameras are used for three-dimensional object recognition in visual servoing. In the thruster system of ROV, 4 vectored thrusters and 4 vertical thruster are installed. The specifications of main hardware components are summarized in Table 1. The thrust of the vectored thruster acts in the horizontal direction (X_H and Y_H in Fig. 2). The thrust of the vertical thruster acts in the vertical direction (Z_H in Fig. 2).

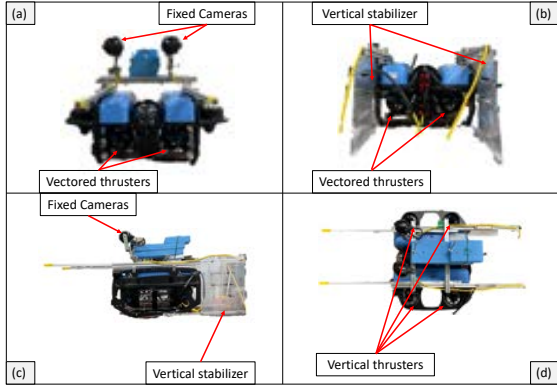


Fig. 8. Overview of ROV: (a) front view, (b) back view, (c) side view, (d) top view.

Table 1. Specification of ROV.

Max : operation depth [m]	100
Dimension [mm]	457 (L) × 338 (W) × 254 (H)
Dry weight [kg]	9-10 (without ballast), 10-11 (with ballast)
Ballast Weight [g]	200 (6 stainless steel weights)
Number of thrusters	4 (vertical), 4 (vectored)
Number of cameras	3 (2 fixed cameras, 1 front camera)
Maximum thrust force [N]	88 (horizontal and traverse), 69 (vertical)
Tether cable [m]	300

Note that the rotation of vehicle is controlled by four vectored thrusters that rotate in opposite direction(ε_3 in Fig. 2).

3. EXPERIMENT OF VISUAL SERVOING

Experiments were conducted in simulated environment in order to verify the effectiveness of the proposed visual servoing. Firstly, the experiment in which the underwater robot keeps the relative pose with fixed target, was conducted while setting the experimental conditions approving that the robot is regulated to the final pose against the target object.

3.1. Experiment Environment

A pool (length×width×height, $2m \times 3m \times 0.75m$) filled with tap water was used as an experimental tank for underwater robot experiments. Based on the images which are given by binocular camera, the pose information is calculated through model-based matching method and RM-GA. The experimental layouts of the recognition experiments are shown in Fig.9. In Fig.9, Σ_H and Σ_M are the coordinate systems of the ROV and 3D marker. In the initial position, The distance between the dual-camera and ROV is set to $(x, y, z) = (600, 0, 0)[mm]$, $\varepsilon_3 = 0[^\circ]$, where $x[mm]$, $y[mm]$, $z[mm]$, $\varepsilon_3[^\circ]$ represent the position and orientation of the target object recognized by GA. In order to regulate the underwater robot with this desired relative pose to the target, the calculated values are output to each thruster.

3.2. Experiment results

Fig.10 shows the time variation of the fitness value at the time of GA recognition of underwater robot that was regulated in $x_d = 600[mm]$, $y_d = 0[mm]$, $z_d = 0[mm]$, $\varepsilon_{3d} = 0[^\circ]$. According to the experiment result, it can be seen that the fitness value is maintained above 0.5. In general, when performing visual servoing, RM-GA recognition accuracy is thought to be necessary 0.4 or more. It seems that the esti-

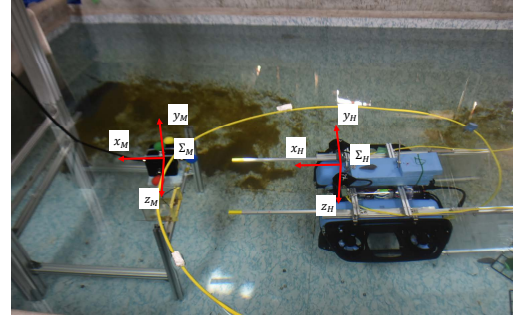


Fig. 9. Experimental environment using passive ROV and 3D marker.

mated position are continuously recognized including large errors from the target values $30 - 40[s]$ and $168 - 175[s]$ for the position in the x -axis direction and around $80[s]$ for the position in the y -axis direction. However, it can be said that it is allowable error range in Visual servoing, because it is understood that it is within the field angle regardless of the error from the photograph of Fig.10 camera images of B, C, D.

4. EXPERIMENT OF DOCKING

The result of the visual servoing experiment, it was proven that the attitude control was possible with the stable fitness. Then, the docking experiment was carried out in the environment equal to the visual servoing experiment.

4.1. docking control sequence

This docking control experiment was performed as shown in (a) to (d), and will be described in detail below.

(a) Visual Servoing step

With a 3D marker in the camera image, the camera follows the target relative position $[x_d, y_d, z_d] = [600, 0, 0]$. The attitude is expressed as a quaternion, and by following $\varepsilon_3 = 0$ with visual servo as a target, the camera is facing the 3D marker. $\varepsilon_1, \varepsilon_2$ is the position about the x_H, y_H . The reason for setting $y_d = 0[mm]$, $z_d = 0[mm]$ is to adjust the offset between the position of the 3D marker and the fitting hole and the positional relationship between the Σ_H origin and the fitting rod. When the state of the error allowance ($|y_d - y| \leq 40[mm]$, $|z_d - z| \leq 40[mm]$, $|\varepsilon_3 - \varepsilon| \leq 5[^\circ]$) continues for a certain period of time in the state where the ROV and the 3D marker are directly paired, it shifts to (c) Docking step.

(b) Docking step

When the $|y_d - y| \leq 40[mm]$, $|z_d - z| \leq 40[mm]$ is satisfied, the ROV advances in the x -axis direction at a speed of $30[mm/s]$ and fits into the fitting hole by time-varying the target value in the depth direction with the $x_d = 600 - 30t[mm]$ (t : when fitting is started, $t = 0[s]$). When x_d reaches the final value of $350[mm]$, the ROV moves to the position where fitting is completed. However, if the fitting condition (The error in the y -axis and z -axis is $\pm 40[mm]$ or less.) is not satisfied halfway, the current time-varying target value in the x -axis direction is fixed and the camera returns to (a) Visual Servoing step.

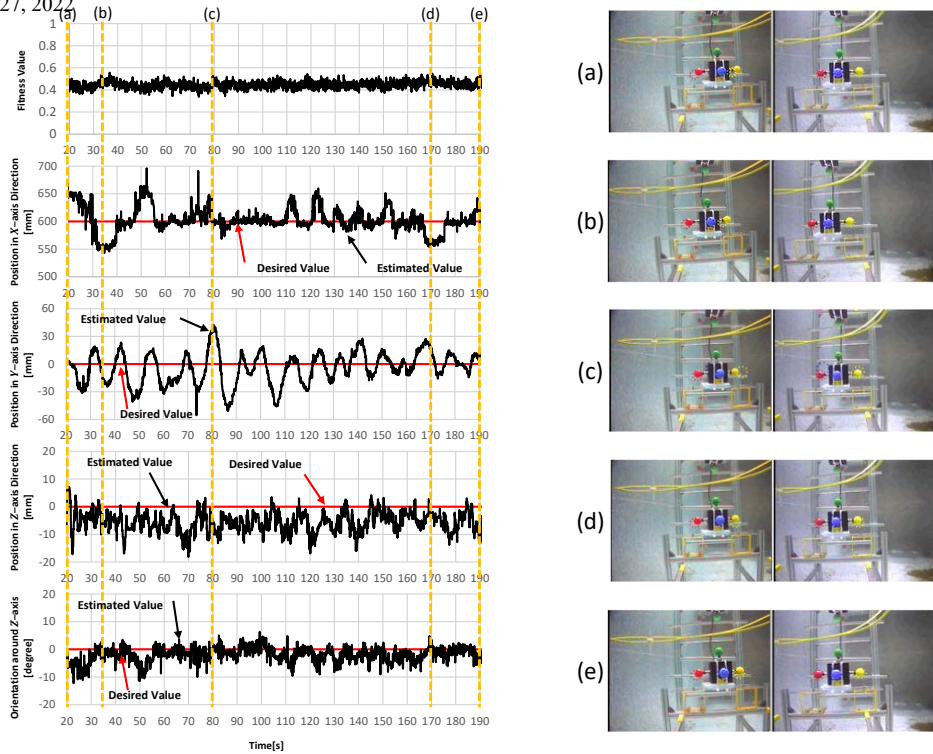


Fig. 10. experiment of visual servoing. The graphs on the left are Fitness value, Position in X, Y, and Z-axis Direction, and Orientation around Z-axis from the top. Right column shows the camera images from ROV, where (a) to (e) corresponded to the time indicated by (a) to (e) shown in left hand side time profiles of docking datum.

(c) Docking Completion step

In this state, as in the Visual Servoing state, the 3D marker is controlled to maintain a certain relative position and attitude ($[x_d, y_d, z_d] = [600, 0, 0][mm], \varepsilon_{3d} = 0[^\circ]$).

(d) Launching step

If the controllable fitness of fit is maintained, the process shifts to (d) Launching step. In order to return to the initial position completely, the target value is gradually changed and returned.

4.2. Experiment results

Fig.11 shows the distance between the ROV and the 3D marker and the RM-GA goodness of fit over time in 10 consecutive docking experiments. There was no significant difference in the docking time of 10 times, and the each docking from start to finish took an average of about 100[s]. Next, the results of the seventh docking experiment out of 10 consecutive docking experiments are shown in fig.12. The graph on the left in Fig.12 shows the fitness value, position in the x, y, and z directions, and angle in the z axis rotation direction as time profiles. The right side of Fig.12 is a camera image of an elapsed time point from (a) to (f) in the graph. (a) indicates when the sixth experiment was completed, (b) indicates when the underwater robot returned to the initial position, (c) indicates when docking started, (d) indicates when the target value of the underwater robot became the docking point, (e) indicates when the estimated value of the underwater robot became the docking point, and (f) indicates when docking was completed. It can be said that the docking condition was easily satisfied, because in the docking, the position in each direction followed the target value, and it was within the error tolerance. However, there is an instant in the z-axis direction which is outside the error tolerance. This may be caused by

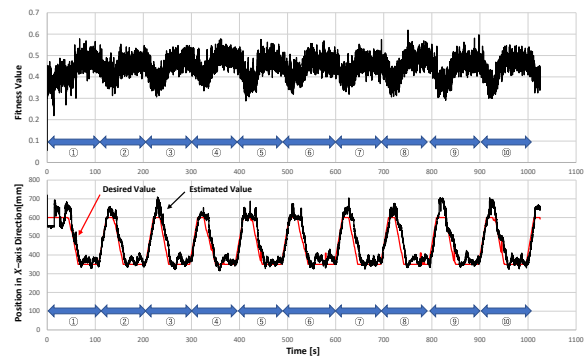


Fig. 11. Experiment of 10 times continuous docking in the pool. The graphs are Fitness value and Position in X-axis Direction. The numbers represent the lengths of the first to tenth docking experiments, respectively.

insufficient evolution of RM-GA. Therefore, it was proven that countermeasures such as increasing the evolution number of RM-GA were necessary.

5. CONCLUSION

It was confirmed that visual servoing experiment and docking experiment were possible using newly introduced underwater robot. As future development, the research of more advanced autonomous underwater robot is advanced by improvement of evolution part in RM-GA and remodeling of ROV to AUV.

REFERENCES

[1] F. Chaumette and S. Hutchinson, "Visual servo control I: Basic approaches," IEEE Robot. Autom. Mag., Vol.13, No.4, pp. 82-90, Dec. 2006.

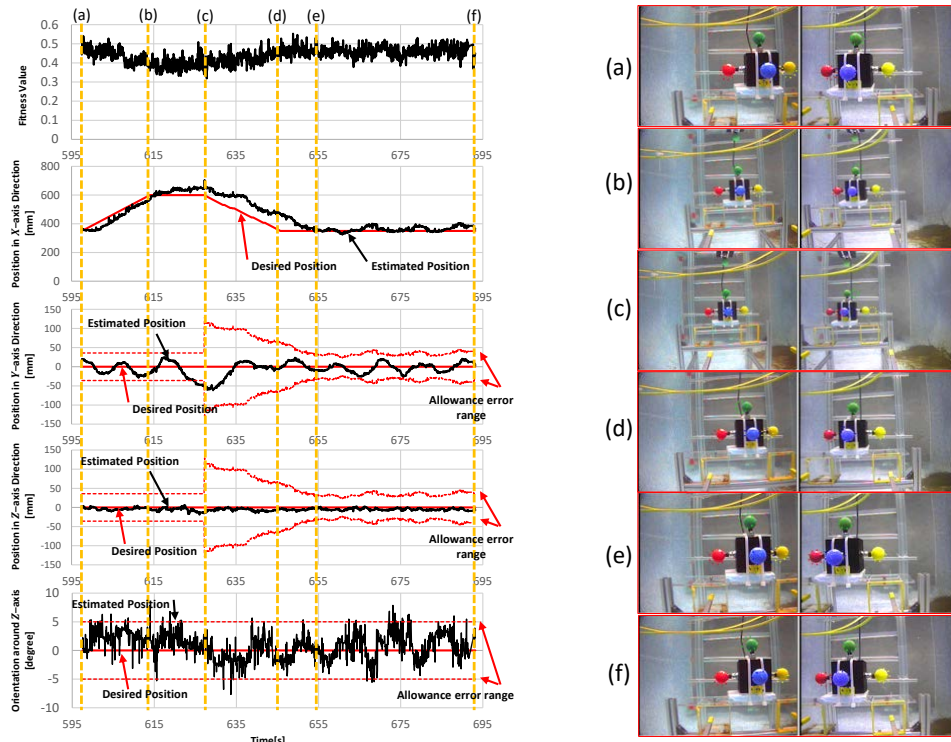


Fig. 12. This is the 7th of 10 consecutive docking experiments in the pool. The graphs on the left are Fitness value, Position in X , Y , and Z -axis Direction, and Orientation around Z -axis from the top. Right column shows the camera images from ROV, where (a) to (f) corresponded to the time indicated by (a) to (f) shown in left hand side time profiles of docking datum.

[2] F. Chaumette and S. Hutchinson, "Visual servo control II: Advanced approaches," *IEEE Robot. Autom. Mag.*, Vol.14, No.1, pp. 109-118, Mar. 2007.

[3] F. Janabi-Sharifi, L. Deng, and W. J. Wilson, "Comparison of basic visual servoing methods," *IEEE/ASME Trans. on Mechatronics*, Vol.16, No.5, October 2011..

[4] Y. Okuda, H. Kamada, S. Takahashi, S. Kaneko, K. Kawabata, and F. Takemura, "Method of dynamic image processing for ecology observation of marine life," *J. of Robotics and Mechatronics*, Vol.25, No.5, pp. 820-829, 2013.

[5] D. Lee, X. Tao, H. Cho, and Y. Cho, "A dual imaging system for flip-chip alignment using visual servoing," *J. of Robotics and Mechatronics*, Vol.18, No.6, pp. 779-786, 2006.

[6] G. L. Foresti, S. Gentili, and M. Zampato, "A vision-based system for autonomous underwater vehicle navigation," *OCEANS '98 Conf. Proc.* (Vol.1), pp. 195-199, 1998.

[7] J.-Y. Park, B.-H. Jun, P.-M. Lee, and J. Oh, "Experiments on vision guided docking of an autonomous underwater vehicle using one camera," *Ocean Eng.*, Vol.36, No.1, pp. 48-61, Jan. 2009.

[8] T. Ura, Y. Kurimoto, H. Kondo, Y. Nose, T. Sakamaki, and Y. Kuroda, "Observation behavior of an AUV for ship wreck investigation," *Proc. of the OCEANS 2005 MTS/IEEE Conf.*, Vol.3, pp. 2686-2691, 2005.

[9] N. Palomeras, P. Ridao, D. Ribas, and G. Vallicrosa, "Autonomous I-AUV docking for fixed-base manipulation," *Preprints of the Int. Federation of Automatic Control*, pp. 12160-12165, 2014.

[10] S. Sagara, R. B. Amber, and F. Takemura, "A stereo vision system for underwater vehicle-manipulator system - proposal of a novel concept using pan-tilt-slide cameras -," *J. of Robotics and Mechatronics*, Vol.25, No.5, pp. 785-794, 2013.

[11] Y. Li, Y. Jiang, J. Cao, B. Wang, and Y. Li, "AUV docking experiments based on vision positioning using two cameras," *Ocean Engineering*, Vol.110, pp. 163-173, December 2015.

[12] F. Maire, D. Prasser, M. Dunbabin, and M. Dawson, "A vision based target detection system for docking of an autonomous underwater vehicle," *Australasian Conf. on Robotics and Automation (ACRA)*, Sydney, Australia, December 2-4, 2009.

[13] S. Ishibashi, "The stereo vision system for an underwater vehicle," *Oceans 2009, Europe, Bremen*, pp. 1343-1348, 2009.

[14] S. Cowen, S. Briest, and J. Dombrowski, "Underwater docking of autonomous undersea vehicle using optical terminal guidance," *Proc. IEEE Oceans Engineering*, Vol.2, pp. 1143-1147, 1997.

[15] K. Teo, B. Goh, and O. K. Chai, "Fuzzy docking guidance using augmented navigation system on an AUV," *IEEE J. of Oceans Engineering*, Vol.37, No.2, April 2015.

[16] M. D. Feezor, F.Y. Sorrell, P. R. Blankinship, and J. G. Bellingham, "autonomous underwater vehicle homing/docking via electromagnetic guidance," *IEEE J. of Oceans Engineering*, Vol.26, No.4, pp. 515-521, October 2001.

[17] R. S. McEwen, B.W. Hobson, L. McBride, and J.G. Bellingham, "Docking Control System for a 54-cm-Diameter (21-in) AUV," *IEEE J. of Oceans Engineering*, Vol.33, No.4, pp. 550-562, October 2008.

[18] K. Teo, E. An, and P.-P. J. Beaujean, "A robust fuzzy autonomous underwater vehicle (AUV) docking approach for unknown current disturbance," *IEEE J. of Oceans Engineering*, Vol.37, No.2, pp. 143-155, April 2012.

[19] J.-Y. Park, B.-H. Jun, P.-M. Lee, F.-Y. Lee, and J.-h. Oh, "Experiment on underwater docking of an autonomous underwater vehicle 'ISiMI' using optical terminal guidance," *IEEE Oceanic Engineering, Europe*, pp. 1-6, 2007.

[20] A. Negre, C. Pradalier, and M. Dunbabin, "Robust vision-based underwater homing using self similar landmarks," *J. of Field Robotics*, Wiley-Blackwell, Special Issue on Field and Service Robotics, Vol.25, No.6-7, pp. 360-377, 2008.

[21] M. Dunbabin, B. Lang, and B. Wood, "Vision-based docking using an autonomous surface vehicle," *IEEE Int. Conf. on Robotics and Automation*, Pasadena, CA, USA, 2008.

[22] P. Batista, C. Silvestre, and P. Oliveira, "A two-step control strategy for docking of autonomous underwater vehicles," *American Control Conf.*, Fairmont Queen Elizabeth, Montreal, Canada, 2012.

[23] N. Palomeras, A. Penalver, M. Massot-Campos, G. Vallicrosa, P. L. Negre, J. J. Fernandez, P. Ridao, P. J. Sanz, G. Oliver-Codina, and A. Palomer, "I-AUV docking and intervention in a subsea panel," *IEEE/RSSJ Int. Conf. on Intelligent Robots and Systems*, Chicago, IL, pp 2279-2285, 2014

[24] S.-C. Yu, T. Ura, T. Fujii, and H. Kondo, "Navigation of autonomous underwater vehicles based on artificial underwater landmarks," *OCEANS MTS/IEEE Conf. and Exhibition*, Vol.1, pp. 409416, 2001.

[25] M. Myint, K. Yonemori, A. Yanou, K.N. Lwin, M. Minami, and S. Ishiyama, "Visual Servoing for Underwater Vehicle Using Dual-Eyes Evolutionary Real-Time Pose Tracking", *Journal of Robotics and Mechatronics* Vol.28 No.4, 2016.

[26] W. Song, M. Minami, and S. Aoyagi, "Feedforward on-line pose evolutionary recognition based on quaternion," *J. of the Robot Society of Japan*, Vol.28, No.1, pp. 55-64, 2010 (in Japanese).

[27] W. Song and M. Minami, "On-line motion-feedforward pose recognition invariant for dynamic hand-eye motion," *IEEE/ASME Int. Conf. on Advanced Intelligent Mechatronics*, pp. 1047-1052, 2008.

[28] W. Song and M. Minami, "Stability/precision improvement of 6-DoF visual servoing by motion feedforward compensation and experimental evaluation," *IEEE Int. Conf. on Robotics and Automation*, pp. 722-729, 2009.

[29] W. Song and M. Minami, "Hand and eye-vergence dual visual servoing to enhance observability and stability," *IEEE Int. Conf. on Robotics and Automation*, pp. 714-721, 2009.

[30] H. Hsu, Y. Toda, K. Watanabe, M. Minami, "Visibility improvement in relation with turbidity and distance and application to docking", *Artificial Life and Robotics*, Vol.25, No. 3, pp. 453-465, 2020.